Measurement method for determining the magnetic hysteresis effects of reluctance actuators by evaluation of the force and flux variation

AIP | Review of Scientific Instruments

Measurement method for determining the magnetic hysteresis effects of reluctance actuators by evaluation of the force and flux variation

N. H. Vrijsen, J. W. Jansen, J. C. Compter, and E. A. Lomonova

Citation: Rev. Sci. Instrum. **84**, 075003 (2013); doi: 10.1063/1.4813278
View online: http://dx.doi.org/10.1063/1.4813278
View Table of Contents: http://rsi.aip.org/resource/1/RSINAK/v84/i7
Published by the AIP Publishing LLC.

Measurement method for determining the magnetic hysteresis effects of reluctance actuators by evaluation of the force and flux variation

N. H. Vrijsen,[a] J. W. Jansen, J. C. Compter, and E. A. Lomonova
Electromechanics and Power Electronics, Department of Electrical Engineering, Eindhoven University of Technology, Eindhoven, The Netherlands

(Received 20 July 2012; accepted 24 June 2013; published online 16 July 2013)

A measurement method is presented which identifies the magnetic hysteresis effects present in the force of linear reluctance actuators. The measurement method is applied to determine the magnetic hysteresis in the force of an E-core reluctance actuator, with and without pre-biasing permanent magnet. The force measurements are conducted with a piezoelectric load cell (Kistler type 9272). This high-bandwidth force measurement instrument is identified in the frequency domain using a voice-coil actuator that has negligible magnetic hysteresis and eddy currents. Specifically, the phase delay between the current and force of the voice-coil actuator is used for the calibration of the measurement instrument. This phase delay is also obtained by evaluation of the measured force and flux variation in the E-core actuator, both with and without permanent magnet on the middle tooth. The measured magnetic flux variation is used to distinguish the phase delay due to magnetic hysteresis from the measured phase delay between the current and the force of the E-core actuator. Finally, an open loop steady-state ac model is presented that predicts the magnetic hysteresis effects in the force of the E-core actuator. © *2013 AIP Publishing LLC*. [http://dx.doi.org/10.1063/1.4813278]

I. INTRODUCTION

Accurate force prediction of electromechanic actuators is a major issue for high-precision applications. For example, in the semiconductor lithography, these high accuracies are required to operate in the nanometer range. Simultaneously, the desired bandwidth of high-precision actuators is increasing. Because of the accuracy, preferably highly linear voice-coil actuators[1–5] are applied instead of nonlinear reluctance actuators.[6–16] Nevertheless, reluctance actuators are able to achieve a more than 10 times higher force density than voice-coil actuators.[17]

Until now, reluctance actuators are scarcely applied in high-precision applications because of the nonlinear magnetic hysteresis introduced by the soft-magnetic material. Generally, a linear current-force relation is desired. However, ferromagnetic hysteresis results in a nonlinear, history dependent, and rate-dependent relation between the current and the magnetic flux. This flux is directly related to the force and hence, the current-force relation is nonlinear.

Ferromagnetic hysteresis models have been researched for years.[18–20] These research contributions frequently focus on mathematical models predicting magnetic hysteresis in thin films, soft-magnetic toroids or strips. Additionally, hysteresis models are applied to model ferroelectric hysteresis present in piezoelectric actuators.[21–24] However, rarely are experiments performed on reluctance actuators. The few research contributions that include magnetic hysteresis in the analysis of reluctance actuators use time consuming numerical methods, which are not feasible for feed-forward control purposes.[14,25] Moreover, these models are valid for relatively low frequency excitations only and no pre-biasing permanent magnet is included.

In this paper, a measurement method is proposed which is able to identify the magnetic hysteresis effects in the force of an E-core reluctance actuator, both with and without pre-biasing permanent magnet. Furthermore, the used frequency range is between 40 and 480 Hz, and hence includes the dynamic behavior of eddy currents. Additionally, the measurement method is applied to obtain the phase delay due to magnetic hysteresis. This delay is used in an analytical actuator model that can serve the purpose of a feed-forward control method for reluctance actuators. The force measurement instrument is shown schematically in Fig. 1. The E-shaped core of the actuator is mounted on top of the load cell, which is fixed in a cylindrical aluminum frame. The mover of the E-core is fixed to the frame cover. The measured force is linearly related to the output voltage U_F of the charge amplifier. A sinusoidal current excitation is applied to the primary coil while simultaneously the flux through one of the outer teeth is measured with a secondary coil.

II. E-CORE RELUCTANCE ACTUATOR AND EXPERIMENTAL INSTRUMENT

The E-core reluctance actuator under investigation is constructed from laminated SiFe sheets to limit eddy current effects. The E-core actuator is evaluated without and with pre-biasing permanent magnet placed on the middle toot. The middle tooth is shorter than the outer teeth and the tooth area is twice the area of each outer teeth, as schematically illustrated in Fig. 2(a).

An E-core reluctance actuator typically behaves quadratically with current and position. This nonlinear current-force and position-force relation is modeled with a non-hysteretic magnetic equivalent circuit (MEC) model.[26,27] This non-hysteretic actuator model predicts the force of the E-core

[a]Electronic mail: n.h.vrijsen@tue.nl.

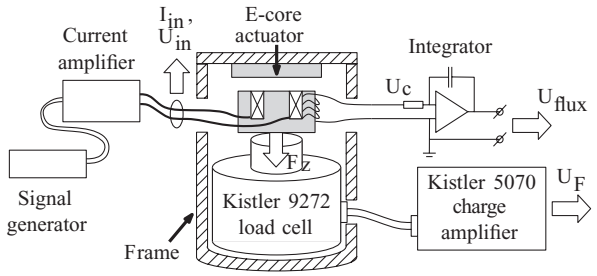

FIG. 1. Measurement instrument (load cell, frame, and charge amplifier), the E-core reluctance actuator, the current amplifier, and the integrator of the magnetic flux.

without and with permanent magnet with an accuracy of 98.5% and 98.7%, respectively. However, for high-precision applications the accuracy of the force prediction for feed-forward control must be improved. Therefore, a measurement method is presented, which distinguishes the phase delay due to magnetic hysteresis effects from the non-hysteretic behavior of the actuator.

A. Non-hysteretic reluctance actuator model

The non-hysteretic analytical actuator model is based on the MEC method. A MEC model is a representation of the magnetic flux paths in the actuator with reluctances $\mathcal{R}$ as the magnetic equivalent to resistances in an electric circuit. The reluctances are used to determine the magnetic flux variation in the actuator. This magnetic flux $\phi(z)$ is directly related to the force produced by an E-core reluctance actuator with permanent magnet. The force is given by three terms,

$$F_z(t) = \frac{N_1 i(t)}{2}\frac{d\phi_{coil}(z)}{dz} + \frac{H_c l_{pm}}{2}\frac{d\phi_{pm}(z)}{dz} + N_1 i(t)\frac{d\phi_{pm}(z)}{dz}, \quad (1)$$

with $i(t)$ the current, N_1 the number of turns of the excitation coil, and z the airgap length. The second and third terms represent the contribution of the permanent magnet, with l_{pm} the length and H_c the coercive field strength of the permanent magnet. The magnetic flux of the excitation coil $\phi_{coil}(z)$ and permanent magnet $\phi_{pm}(z)$ are both dependent on the magnetic circuit, which is modeled with the MEC method including leakage and fringing effects,[26] as visualized in Fig. 2(b). The calculated force of the E-core with permanent magnet is shown in Fig. 3, as a function of the airgap length and excitation current. This calculated force profile is in good agreement with measurements for various airgap lengths and for a range of current excitations. However, the MEC model is limited to an ideal representation of the soft-magnetic iron and hence does not take into account magnetic hysteresis effects.

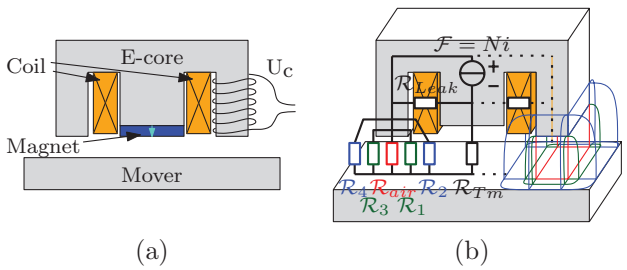

FIG. 2. (a) Schematic illustration of the E-core reluctance actuator with permanent magnet and magnetic flux sensing coil around the right tooth and (b) airgap and leakage permeance as used in the MEC model for the E-core actuator without permanent magnet.

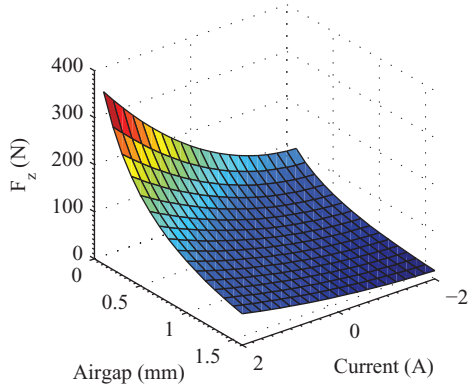

FIG. 3. Calculated force with variable current and variable airgap.

B. Hysteresis model

A hysteresis model with a complex impedance is presented to improve the accuracy of the feed-forward control of an E-core reluctance actuator. An easy and fast model is preferred to a complicated but slightly more accurate hysteresis model for control purposes. Therefore, the elliptic behavior of minor loops in a non-saturated actuator is translated to a complex impedance model (representing the magnetic hysteresis effects). The resultant of the complex impedance model is a rate-dependent phase delay between the current and the modeled force. This hysteresis model does not model any physical representation of magnetic hysteresis, though shows good agreement with the hysteresis measured in the force of the non-saturated E-core reluctance actuator, as will be shown later in Sec. VII. A non-saturated actuator is generally a reasonable assumption, since reluctance actuators are frequently designed for a peak-force that is much higher than the nominal force, while the peak-force is physically limited by the saturation of the iron.

To confirm that the iron in the actuator is not saturated, measurements are performed on a laminated toroid of the same material as the SiFe E-core actuator. A toroidal construction is considered to comply with the IEC 60404-4 standard for measurements on soft-magnetic materials. The measured magnetic hysteresis in a laminated toroid is depicted in Fig. 4 for frequencies within a range of 40–480 Hz and a maximum magnetic flux density of 0.4, 0.8, and 1.2 T. This figure shows a nearly elliptic B-H relation for the minor loops, which grow in width for an increasing frequency. The magnetic field strength H is translated to the excitation current of the E-core actuator, and no saturation is reached for a current up to approximately 3 A-pp, while the measurements on the E-core actuator are performed up to 1.4 A-pp.

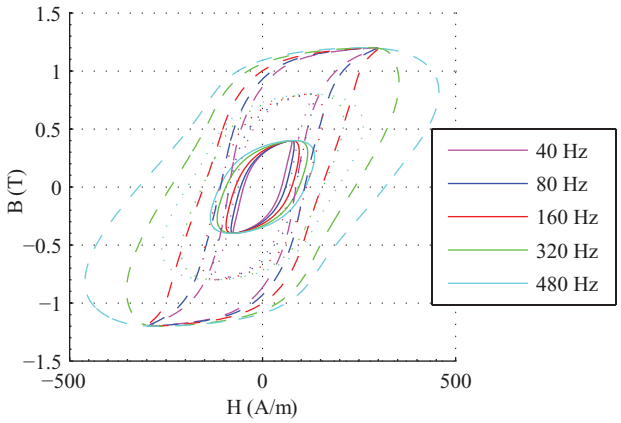

FIG. 4. Magnetic hysteresis and eddy currents measured on a toroid, for $B_{max} = 0.4$ T (solid), $B_{max} = 0.8$ T (dotted), and $B_{max} = 1.2$ T (dashed).

C. Magnetic flux measurement

The Maxwell stress tensor method[13] states that the force is directly related to the squared magnetic flux density in the airgap. Therefore, theoretically a perfect flux measurement can be used to predict the actuator force directly. However, leakage and fringing fluxes are dependent on the airgap length and sizes of the configuration, and hence, the ratio of the measured flux and the flux contributing to the force, changes with position.[28] Even with a constant airgap it is rather difficult to measure the exact leakage and fringing effects.[29]

The flux measurements are performed by means of a coil around one tooth of the E-core actuator, as shown in Fig. 2(a). Only the phase delay of the measured flux with respect to the measured current and force are used in the proposed hysteresis model, to obtain the phase delay due to magnetic hysteresis. The phase angle of the flux is independent of the airgap length and coil positioning. The flux measurement is not used to predict the force because the accuracy of the non-hysteretic actuator model is better than the force calculated from the measured flux.

The voltage, U_c, of the flux coil with $N_2 = 10$ windings is integrated with a low-noise high-bandwidth operational amplifier (NE5534) to obtain the magnetic flux Φ through the coil. The sensing voltage can be expressed as

$$U_c = -N_2 \frac{d\Phi}{dt}. \tag{2}$$

The time delay of the measured magnetic flux density with respect to the force is proportional to the phase delay of the load cell, frame, and charge amplifier. The phase delay between two measured signals is obtained by the maximum of the covariance function given by

$$\sigma_{XY} = \mathrm{cov}(X, Y) = \frac{1}{N}\sum_{i=1}^{N}(x_i - \overline{x})(y_i - \overline{y}), \tag{3}$$

where X is substituted by the force F_z and Y by one period of the squared flux Φ^2 or flux Φ for the E-core actuator without and with permanent magnet, respectively. The measured flux variation is directly related to the force for the actuator with pre-biasing permanent magnet because of a unidirectional flux. While for the actuator without permanent magnet, the flux is bi-directional and the force is unidirectional, which results in a quadratic flux-force relation. The maximum of the covariance gives the delay in time samples, from which the phase delay is calculated with the known sample time and excitation frequency.

D. Force measurement

The measurement instrument consists of a piezoelectric load cell, an aluminum frame (in which the load cell and actuator are mounted), and a Kistler charge amplifier. A schematic illustration of the measurement instrument including the current amplifier and integrator of the magnetic flux, is shown in Fig. 1. The force measurements are performed with the piezoelectric load cell (Kistler type 9272) because it has a high rigidity and hence, a high natural frequency.[30,31] Similar load cells are regularly applied for force and torque measurements of drilling and cutting machines due to the linearity over a large amplitude range.[32,33] Other commonly used passive load cells are the strain gauge/gage[34] and hydrostatic sensor. However, both have lower bandwidth, lower strain sensitivity (factor 1000), and lower rigidity,[30] which results in a larger airgap variation. Disadvantages of piezoelectric load cells are the inability to measure statically over a longer period of time and hence, only steady-state ac measurements are evaluated. Moreover, ferroelectric hysteresis is present in a piezoelectric element,[21–24] which is comparable to ferromagnetic hysteresis effects in a reluctance actuator. However, the Kistler load cell uses the charge-force relation, which is non-hysteretic,[23,24] because it is an electric equivalent of the magnetic flux-force relation for reluctance actuators.

III. MEASUREMENT METHOD

The measurement method is used to distinguish the phase delay due to magnetic hysteresis from the phase delay of the measurement instrument (load cell, frame, and charge amplifier). Two measurements are compared for the identification of the phase delay of the measurement instrument. First, the measured current and force of a voice-coil actuator are analyzed. Second, the current, force, and magnetic flux of the E-core reluctance actuator are measured and analyzed. The block diagram of Fig. 5 summarizes the performed measurements used to identify the phase response of the measurement instrument and finally the phase delay of the E-core actuator due to magnetic hysteresis. The transfer function in the frequency domain of a general force measurement is given by

$$H_{tot}(j\omega) = H_{instr}(j\omega) \cdot H_{act}(j\omega). \tag{4}$$

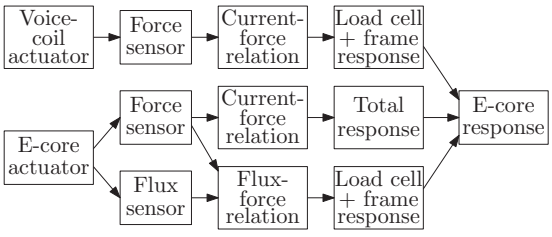

FIG. 5. Block diagram of the proposed measurement method.

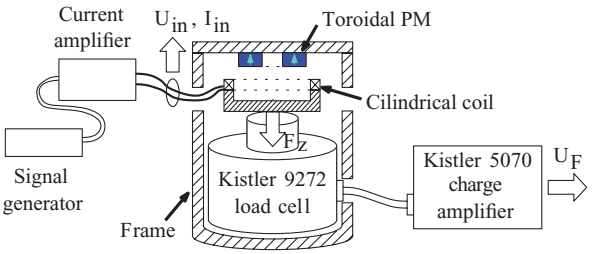

FIG. 6. Measurement instrument (load cell, frame, and charge amplifier) and the voice-coil actuator with the Ferrite magnet.

The measured phase delay between the current and force, $\theta_{meas} = \arg(H_{tot}(j\omega))$, consists of a phase delay introduced by the measurement instrument θ_{instr} and a phase delay introduced by the actuator θ_{act} under investigation. For the E-core actuator, the phase delay is caused by magnetic hysteresis and eddy currents, $\theta_{act} = \theta_{hyst}$. While, for a voice-coil actuator with a ferrite permanent magnet, hysteresis and eddy currents are negligible and hence, $\theta_{act} = 0^\circ$. Hence, the phase response of the load cell, frame, and charge amplifier, θ_{instr}, can be obtained with a voice-coil actuator, as presented in Sec. IV. Additionally, magnetic flux and force measurements of the E-core actuator without and with permanent magnet are shown in Secs. V and VI, respectively. The flux variation of the E-core actuator is used to obtain the phase delay of the measurement instrument. Nonetheless, a full frequency response of the measurement instrument cannot be obtained with flux measurements on a reluctance actuator, because of the quadratic current-force relation.

IV. IDENTIFICATION OF THE FORCE MEASUREMENT INSTRUMENT

The first step of the measurement method is the identification of the force measurement instrument. The frame of the measurement instrument is constructed such that the mechanical resonance occurs around 4.5 kHz, which is much higher than the measuring range (40–480 Hz). The frequency response of the load cell, frame, and charge amplifier is measured with a voice-coil actuator. Figure 6 schematically shows the force measurement instrument with a voice-coil actuator mounted on the piezoelectric load cell.

A. Voice-coil configurations

The measurement instrument is identified with a voice-coil actuator with a ferrite magnet, for which magnetic hysteresis effects are negligible. Magnetic hysteresis and eddy currents are insignificant for this voice-coil actuator, because the change of the magnetic flux in the permanent magnets is minimal, no iron material is used and the electrical resistivity of ferrite is relatively high (ρ = 1–100 Ωm).[35] The frequency response is also measured with a NdFeB and a SmCo permanent magnet, for which the electrical resistivity is orders of magnitudes lower ($\rho = 1.4 \times 10^{-6}$ Ωm and $\rho = 7 \times 10^{-7}$ Ωm, respectively) and hence, eddy currents are significantly present in these two permanent magnets. The same coil is used for all three permanent magnets. The eddy current in the coil is negligible, because the copper wire diameter is 0.2 mm and the skin depth is 2 mm at 1 kHz.

B. Frequency response measurement

The frequency response is measured from the current, I_{in}, to the force, F_z of the voice coil actuators. The measured Bode diagram for each permanent magnet is obtained for a frequency range between 0 and 45 kHz, as shown in Fig. 7. Although, the force measurements are performed up to 480 Hz, the frequency response is measured beyond the major resonance frequency to obtain a better fit of the frequency response model. Figure 7(a) shows the measured amplitude response of the voice-coil with the three different permanent magnets. It shows a similar natural resonance frequency for the three permanent magnets, while the amplitude differs due to different magnet shapes and remanence field strengths.

The major difference between the three permanent magnets can be noticed in the corresponding phase responses, which are shown in Figs. 7(b) and 7(c). Figure 7(c) shows the zoomed-in phase response for frequencies between 100 and 4500 Hz. An extra phase delay is caused by eddy currents as measured for both the SmCo and for the NdFeB permanent magnet. For example, compared to the ferrite magnet an extra phase delay of approximately $\theta_{act} = 15^\circ$ is measured at

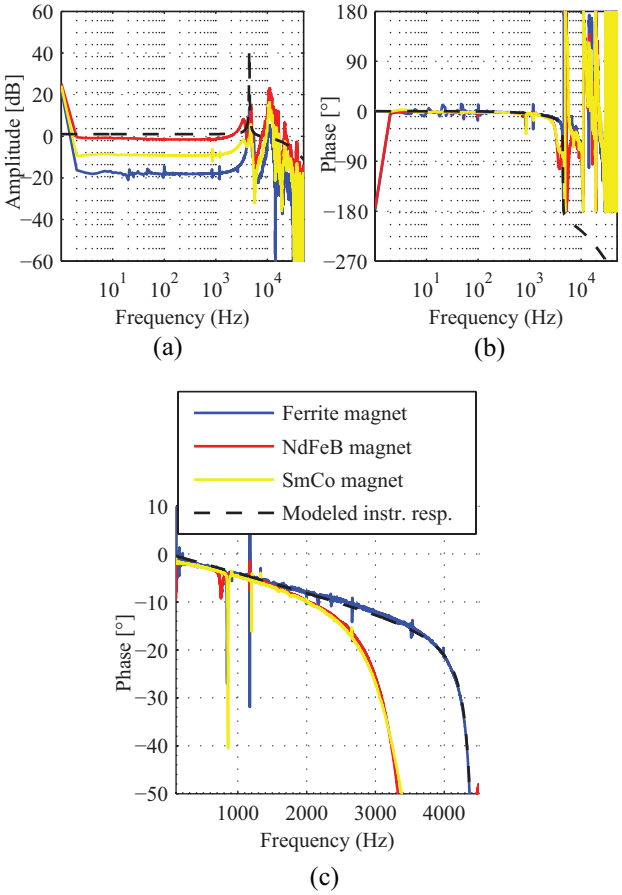

FIG. 7. Bode diagram of the measurement instrument, measured with three different permanent magnets and the modeled instrument response. (a) The amplitude response, (b) the phase response, and (c) the magnified (zoomed) phase response.

3 kHz. This extra phase delay is a result of induced eddy currents in these two permanent magnets. In the ferrite magnet, no extra phase shift is measured, $\theta_{act} \approx 0^\circ$, because of the high electrical resistivity. Therefore, the measured phase response with the ferrite permanent magnet is selected as a benchmark for the frequency response of the measurement instrument. Around 850 and 1175 Hz two peaks are present in Fig. 7(c), which are two additional small resonance peaks. These are out of the measurement range and hence, these are considered irrelevant for the frequency response model.

C. Frequency response model of the measurement instrument

The measured frequency response of the load cell, frame, and charge amplifier is modeled to be able to analytically obtain the phase delay of the measurement instrument, θ_{instr}, in further force measurements. The transfer function of the measurement instrument $H_{instr}(j\omega)$ is split into two transfer functions and each of them is represented by a cascade of two second-order low-pass filters (LPFs), as shown in Fig. 8. The first transfer function $H_{mech}(j\omega)$ describes the mechanical system including the load cell, the frame, and the mounting of the voice-coil actuator, for which the natural resonance is used as identification. The second transfer function $H_{LPF}(j\omega)$ is the LPF of the charge amplifier, which introduces an extra phase delay. The input of the two filters is $X(j\omega)$ and the outputs of the mechanical system and the charge amplifier are $Y_1(j\omega)$ and $Y_2(j\omega)$, respectively.

From the measurements with the ferrite permanent magnet, the undamped natural resonance frequency is obtained as $f_n = 4.45$ kHz and the damping ratio $\zeta_n = 0.012$, which define the filter characteristic of the mechanical system $H_{mech}(j\omega)$. The frequency response of the charge amplifier is obtained from the data sheets and is modeled by a second-order LPF $H_{LPF}(j\omega)$ with a cut-off frequency $f_0 = 31$ kHz and a damping ratio $\zeta_0 = 1$. The modeled phase response of each LPF and the resulting total response of the measurement instrument are shown in Fig. 9 over the frequencies between 100 and 4500 Hz. The phase delay resulting from the LPF of the charge amplifier is dominant for low frequencies, while around the resonance frequency the phase response of the mechanical system rapidly decreases 180°. The modeled instrument response is compared to the measurements in Fig. 7 and shows good agreement with the phase response of the voice-coil actuator with ferrite magnet. The modeled phase response is used to distinguish the phase delay due to magnetic hysteresis from the phase delay of the load cell, frame, and charge amplifier as described by Eq. (4).

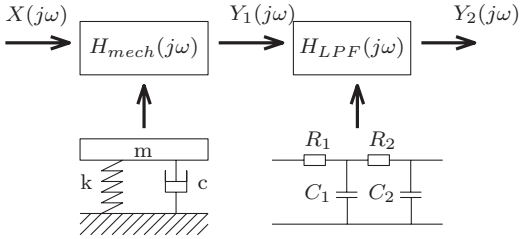

FIG. 8. The low-pass filter model describing the frequency response of the load cell, frame, and charge amplifier.

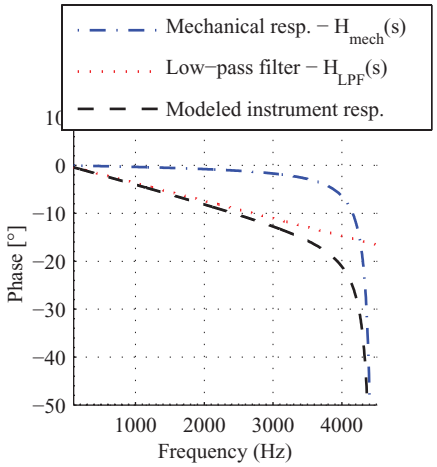

FIG. 9. The modeled phase response of the load cell, frame, and charge amplifier, θ_{instr}.

V. MEASUREMENT RESULTS E-CORE WITHOUT PERMANENT MAGNET

Despite the fact that the E-core is designed to be used with a pre-biasing permanent magnet, the proposed measurement method is first evaluated for the E-core without permanent magnet. The E-core without permanent magnet uses the same core as the E-core with permanent magnet, and hence the middle airgap is larger than the outer airgaps. The force density of this actuator topology is not optimal because of a relatively large effective airgap with respect to the mechanical clearance. The E-core actuator is examined for a constant airgap and excited with a sinusoidal current with a peak-to-peak value of 1.27 A and for a frequency range of 40–320 Hz.

Figure 10(a) shows the measured current-force relation compared to the non-hysteretic analytical actuator model presented in Sec. II. The force error, ΔF, between the analytical

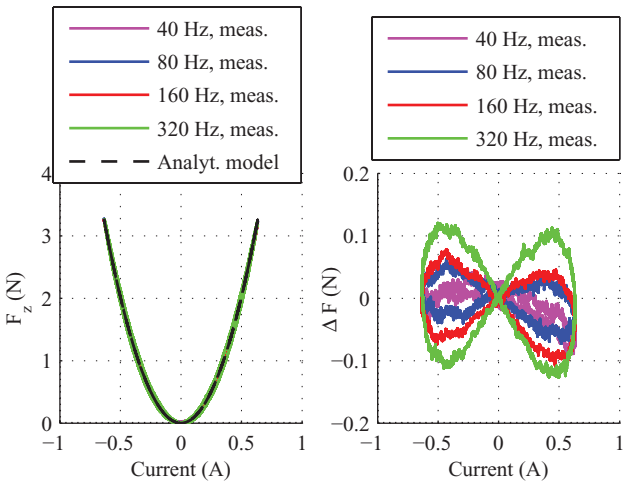

FIG. 10. E-core actuator without permanent magnet. Measured current (a) versus the measured and modeled force F_z, (b) versus the force error ΔF as defined by Eq. (5).

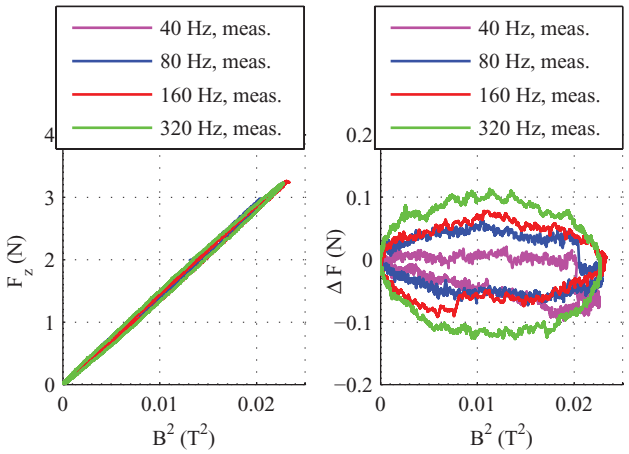

FIG. 11. Measured squared magnetic flux density (B^2) (a) versus the force F_z, (b) versus the force error ΔF.

actuator model and the measurement is shown in Fig. 10(b) and is defined as

$$\Delta F = F_{measured} - F_{analytical}. \tag{5}$$

The loops are caused by two phase delays, namely, due to the measurement instrument and due to magnetic hysteresis effects in the actuator. To distinguish between both phase delays, the measured squared magnetic flux density is plotted against the measured force in Fig. 11(a). Figure 11(b) shows the modeled linear relation subtracted from the measured force. The resulting loops are solely caused by the delay of the measurement instrument, because no magnetic hysteresis is present between the squared magnetic flux density, B^2, and the force, F_z. The phase delay obtained from all these measured loops will be compared later to the phase delay measured with the voice-coil actuator and is shown in Fig. 18.

To isolate magnetic hysteresis effects from the measurements, the phase delay of the measurement instrument must be subtracted from the measurement. Figure 12(a) shows the $(B^2 - F_z)$ relation for a frequency of 320 Hz, with and without a phase correction of $\theta_{instr} = 1.52^\circ$ on the force. The force error, ΔF, that is present after the phase correction of the force

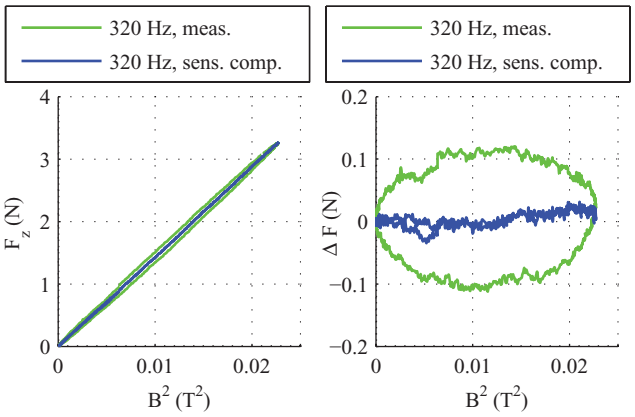

FIG. 12. Measurement with and without phase shift compensation at 320 Hz of the squared magnetic flux density B^2 (a) versus the force F_z and (b) versus the force error ΔF.

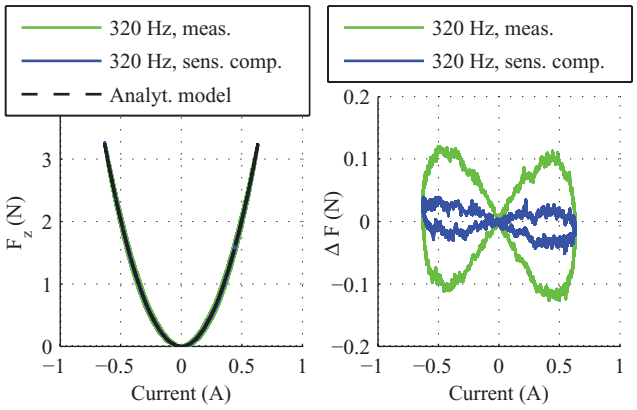

FIG. 13. Measurement with and without phase shift compensation at 320 Hz of the current (a) versus the force F_z and (b) versus the force error ΔF.

is depicted in Fig. 12(b). This phase correction is obtained by means of the covariance as given in Eq. (3). The error for larger magnetic flux densities is a result of a dc-error of the force measurement, which is also distinguishable for the lowest frequencies in Fig. 10(b). The same phase correction as applied in Fig. 12 is applied for the current-force relation, as shown in Fig. 13(a). The error that remains after the phase compensation of the force sensor is shown in Fig. 13(b). It can be stated that the loop after compensation is a result of the magnetic hysteresis and eddy currents in the iron actuator core. The largest remaining force error, ΔF, for an excitation of 320 Hz, is 1.23% of the total force. The force error is smaller for excitations with lower frequencies because less eddy currents are present in that case. Hence, the results for lower frequencies are not shown, because the signal-to-noise ratio is too small to clearly distinguish the force error due to magnetic hysteresis.

VI. MEASUREMENT RESULTS E-CORE WITH PERMANENT MAGNET

The measurement method is now evaluated for the E-core with a permanent magnet placed on the middle tooth. Prebiasing the magnetic flux density with the permanent magnet increases the force range from (0–3.3) N up to a force range of (125–220) N, with a similar current excitation. Besides the higher force range with the permanent magnet, a disadvantage could be an increase of eddy currents, because the permanent magnet is not laminated. For this actuator, sinusoidal excitations of (40, 80, 160, 320, 480) Hz are investigated with a peak-to-peak current of 0.25, 0.5, 1, and 1.4 A-pp. Only the measurements with a peak-to-peak current of 1.4 A are shown in this section, because the magnetic hysteresis and eddy current effects are more distinguishable for larger excitations, as also shown in Fig. 4.

Figure 14(a) shows the nonlinear current-force relation and Fig. 14(b) shows the error between the measured force and the non-hysteretic analytic actuator model. As in Sec. V, the elliptic shapes are a result of two phase delays. The compensation for the phase delay of the measurement instrument for a frequency of 320 Hz, is shown in Fig. 15. The compensated phase shift at 320 Hz is $\theta_{instr} = 1.52^\circ$, as obtained from

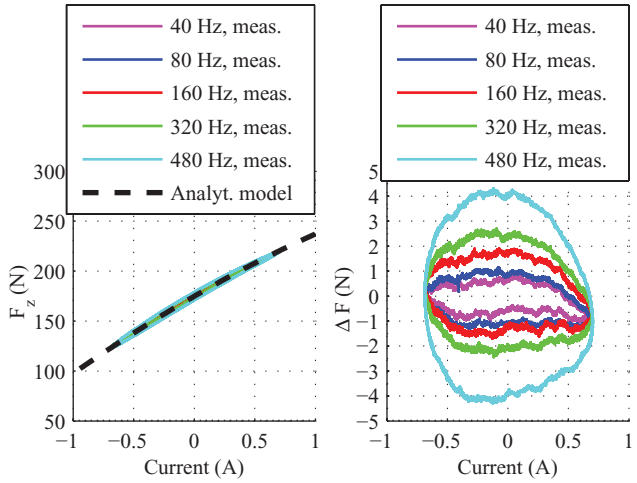

FIG. 14. E-core actuator with permanent magnet. Measured current versus the (a) force F_z and (b) force error ΔF as defined by Eq. (5).

the covariance of the measured force and flux variation. The largest remaining force error between the analytic and measured force, ΔF, for an excitation of 320 Hz is 0.63% of the total force.

The force error due to magnetic hysteresis and eddy currents (after compensation for the measurement instrument) for all evaluated frequencies is shown in Fig. 16. The maximum force error occurs for a current of approximately 0 A and hence, the maximum force error is defined as the height of the loop-eye for a current of 0 A. Figure 17 shows the force error divided by the force range for various frequencies, in percentages. This shows that the magnetic hysteresis and eddy currents do not depend on the excitation amplitude, which can only be the case when the E-core is not saturated (for those excitations).

As explained in Sec. II C, the phase delay between the measured force and magnetic flux of the E-core actuator can be used to obtain the phase delay at the excitation frequency. Therefore, all the measured phase delays between force and magnetic flux of the E-core actuator are compared to the measured and modeled phase responses as shown in Fig. 18. The

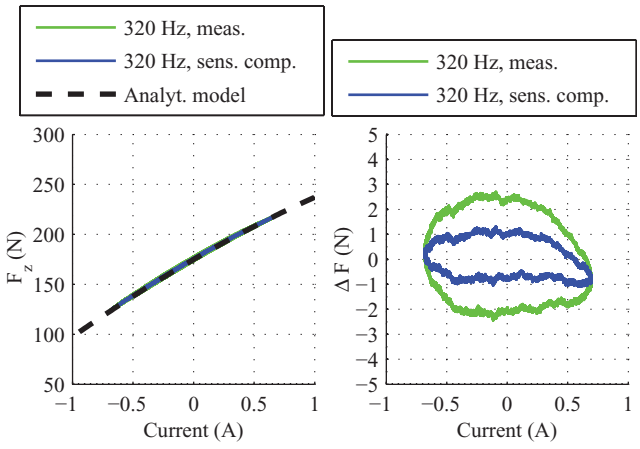

FIG. 15. E-core actuator with permanent magnet. Measured current versus the (a) force F_z and (b) force error ΔF, with and without phase shift compensation at 320 Hz.

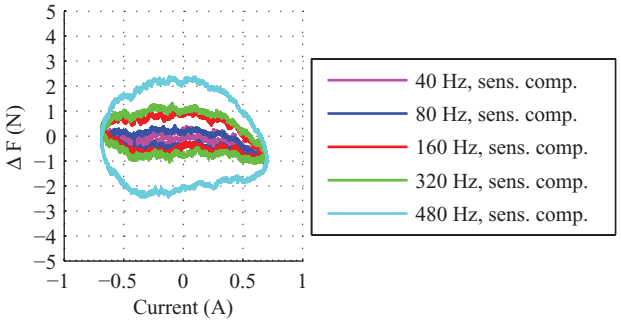

FIG. 16. E-core actuator with permanent magnet. The force error due to hysteresis after compensation for the phase shift of the measurement instrument.

measured phase delays between the force and flux variation are in good agreement with the measured phase responses of the ferrite voice-coil and the low-pass filter model. The phase delays of the E-core actuator without and with permanent magnet are shown for the excitation frequencies (40, 80, 160, 320, 480, 640, 1280) Hz, which are measured for various current amplitudes.

VII. STEADY-STATE AC MAGNETIC HYSTERESIS MODEL

Previous force measurements showed the magnetic hysteresis and eddy current effects, which are present in the force of this E-core reluctance actuator. The magnetic hysteresis effects in the force appear to be similar to the elliptic shape introduced by the phase delay of the measurement instrument. Therefore, a complex impedance model is proposed to predict the effects of the magnetic hysteresis and eddy currents in this E-core actuator. The hysteresis model of the E-core with permanent magnet is given for steady-state ac measurements, as

$$F_z(t) = \frac{N_1}{2} i(\omega t - \theta_{hyst}) \frac{d\phi_{coil}}{dz} + \frac{H_c l_{pm}}{2} \frac{d\phi_{pm}}{dz} + N_1 i(\omega t - \theta_{hyst}) \frac{d\phi_{pm}}{dz}. \quad (6)$$

This equation is similar to Eq. (1), although it now includes an equivalent phase delay, θ_{hyst}, for the current, which represents magnetic hysteresis effects in the E-core actuator. The phase delay due to magnetic hysteresis, θ_{hyst}, can be

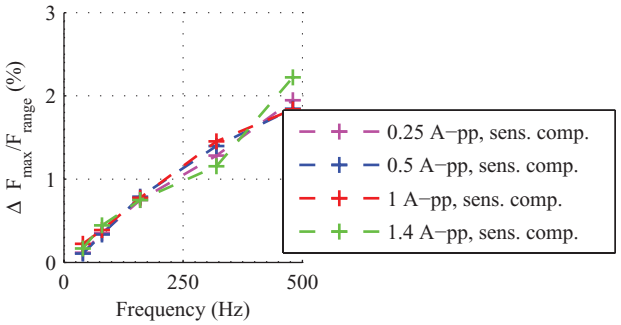

FIG. 17. The maximum force error due to magnetic hysteresis in the E-core actuator with permanent magnet, in percentages of the force range.

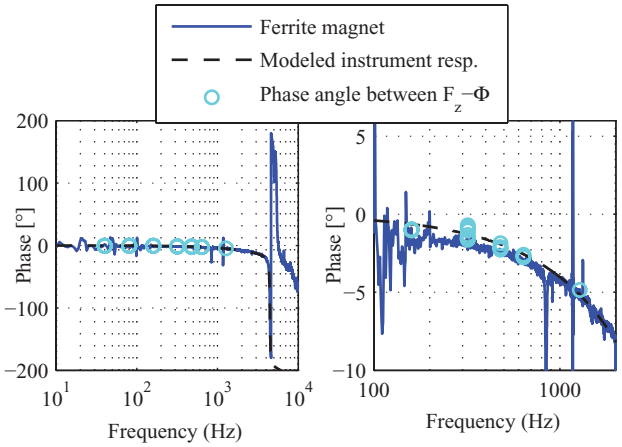

FIG. 18. (a) The modeled phase delay of the load cell, frame, and charge amplifier (Fig. 9) compared to the measured phase delay with the ferrite magnet (Fig. 7), (b) magnified (zoomed) between 100 and 2000 Hz.

obtained by means of the covariance between the current and the measured flux, similar to the method for obtaining the phase delay between the flux and the force presented in Sec. III. In case it is not possible or preferable to perform a flux measurement, the phase delay due to hysteresis can also be calculated with Eq. (4), presuming that the measurement instrument is identified and modeled and hence, θ_{instr} is known.

The equivalent phase delay in the current introduces an elliptic behavior of the force calculated with the non-hysteretic model, Eq. (1). This phase delay model reduces the force error (due to magnetic hysteresis and eddy currents) by a factor 2.5 for the E-core actuator without permanent magnet and a 320 Hz excitation. For the E-core with permanent magnet, the force error predicted with the non-hysteretic force model is reduced by a factor 5 for a 320 Hz excitation. The remaining force error after hysteresis compensation for the actuator without permanent magnet and with permanent magnet are shown in Figs. 19(a) and 19(b), respectively. The amplitude of the force error that is left after hysteresis compensation is of the same order of magnitude as the measurement noise.

The proposed phase delay model reduces the error significantly because the E-core actuator is not saturated. The

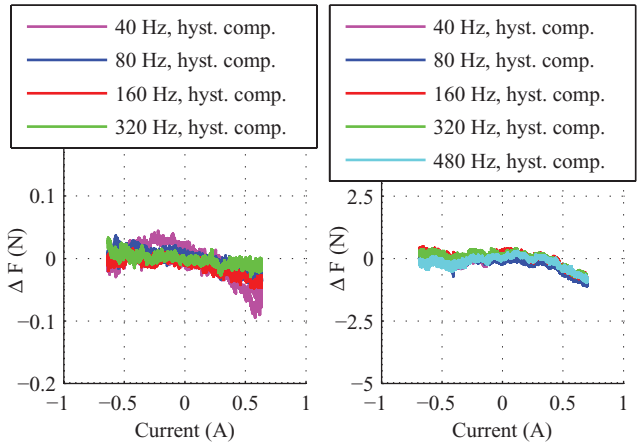

FIG. 19. Force error ΔF after hysteresis compensation. (a) E-core without permanent magnet and (b) E-core with permanent magnet.

presented analytic hysteresis method, is relatively easy compared to frequently applied magnetic hysteresis models, such as Jiles-Atherton[18] or Preisach models,[19,20] which are more demanding regarding computation time. Hence, the phase delay model is considered more suitable for fast feed-forward control of reluctance actuators under a nearly sinusoidal excitation. Note that the model is not applicable for arbitrary input signals, because no dynamic rate-dependencies are taken into account.

VIII. CONCLUSIONS

A measurement method has been presented, which identifies the magnetic hysteresis and eddy current effects occurring in a high-precision E-core reluctance actuator. This method is based on the measurement of the change of the magnetic flux through the soft-magnetic material. The high-bandwidth measurement instrument is identified with a voice-coil actuator. The analysis showed that the force measurement introduces a significant phase delay. The phase delay of the measurement instrument is measured and an equivalent LPF-model is proposed. This model is verified by means of measurements of the magnetic flux variation in the E-core actuator. The phase delay caused by magnetic hysteresis effects in the E-core actuator is obtained by compensation for the phase delay of the measurement instrument. For a frequency of 320 Hz, the non-hysteretic analytical model has an accuracy of 98.5% and 98.7% for the E-core without and with permanent magnet, respectively.

Finally, a phase delay model is presented, which compensates for the phase delay between the current and the force caused by magnetic hysteresis and eddy currents. The proposed measurement method is used to obtain this phase delay due to magnetic hysteresis. For a 320 Hz current excitation, the presented phase delay model reduces the force error with a factor 2.5 and 5 for the actuator without permanent magnet and the actuator with permanent magnet, respectively. The reduction is more significant for the actuator with permanent magnet, because in this case the change of the magnetic flux density is larger. The accuracy of the force prediction with the proposed phase delay model is 99.4% and 99.7% for the actuator without and with permanent magnet, respectively. The remaining force error has a similar magnitude as the noise of the force measurement instrument.

[1] J. Makarovic, M. G. E. Schneiders, A. M. v. d. Wielen, E. A. Lomonova, M. J. G. v. d. Molengraft, R. M. v. Druten, J. C. Compter, M. Steinbuch, and P. H. J. Schellekens, in *Proceedings of the 7th International Conference on Motion and Vibration Control*, 2004.
[2] J. W. Jansen, C. M. M. v. Lierop, E. A. Lomonova, and A. J. A. Vandenput, IEEE Trans. Ind. Appl. **44**(4), 1108–1115 (2008).
[3] W.-J. Kim, D. L. Trumper, and J. H. Lang, IEEE Trans. Ind. Appl. **34**(6), 1254–1262 (1998).
[4] J. C. Compter, P. C. M. Frissen, and J. v. Eijk, U.S. patent 20080203828 A1 (28 Aug 2008).
[5] X. Wu, S. Chen, W. Chen, M. Yang, and W. Fu, Rev. Sci. Instrum. **82**, 105103 (2011).
[6] S. Kudarauskas, *Introduction to Oscillating Electrical Machines* (Publishing office of Klaipeda University (Klaipeda), Klaipeda, Lithuania, 2004).
[7] B. X. S. Alexander, R. Rarick, and L. Dong, in *Proceedings of the American Control Conference, 2007* (IEEE, 2007), pp. 2910–2914.

[8]M. R. A. Calado, A. E. Santo, S. J. P. S. Mariano, and C. M. P. Cabrita, in *Proceedings of the International Conference of POWERENG, 2009* (JSME, 2009), pp. 315–320.
[9]N. C. Cheung, in *Proceedings of the Third International Conference of IPEMC 2000* (International Academic Publishers World Publishing Corporation, 2000), Vol. 2, pp. 832–837.
[10]D. S. B. Fonseca, T. J. B. Godinho, and C. P. Cabrita, in *Proceedings of the ICEM* (IEEE, 2008), pp. 1–6.
[11]J. L. G. Janssen, J. J. H. Paulides, E. A. Lomonova, and A. J. A. Vandenput, in *Proceedings of the Industry Applications Conference, 2007, 42nd IAS Annual Meeting* (IEEE, 2007), pp. 502–509.
[12]C. Weissbacher, H. Stelzer, and K. Hameyer, IEEE/ASME Trans. Mechatron. **15**(4), 615–622 (2010).
[13]E. P. Furlani, *Permanent Magnet and Electromechanical Devices: Materials, Analysis, and Applications* (Academic Press, USA, 2001), pp. 112–116, 270–276.
[14]S. Mittal and C.-H. Menq, IEEE/ASME Trans. Mechatron. **5**(4), 394–409 (2000).
[15]A. F. Bakker, B. C. A. Dirkx, and M. v. Lent, in *Proceedings of the ASPE* (ASPE, 2005).
[16]Z. Ren and L. S. Stephens, IEEE/ASME Trans. Mechatron. **10**(6), 666–674 (2005).
[17]N. H. Vrijsen, J. W. Jansen, and E. A. Lomonova, in *Proceedings of the 14th International Conference of EPE/PEMC, 2010* (IEEE, 2010), pp. S3-29–S3-36.
[18]D. C. Jiles and D. L. Atherton, J. Appl. Phys. **55**(6), 2115–2120 (1984).
[19]I. D. Mayergoyz, J. Appl. Phys. **57**(8), 3803–3805 (1985).
[20]G. Bertotti, *Hysteresis in Magnetism for Physicist, Materials Scientists, and Engineers* (Academic Press, 1998), Vol. 1.
[21]R. Changhai and S. Lining, Rev. Sci. Instrum. **76**, 095111 (2005).
[22]H. Xie, M. Rakotondrabe, and S. Regnier, Rev. Sci. Instrum. **80**, 046102 (2009).
[23]G. Y. Gu and L. M. Zhu, Rev. Sci. Instrum. **81**, 085104 (2010).
[24]A. A. Eielsen, J. T. Gravdahl, and K. Y. Petterson, Rev. Sci. Instrum. **83**, 085001 (2012).
[25]S. Rosenbaum, M. Ruderman, T. Strohla, and T. Bertram, IEEE Trans. Magn. **46**(12), 3984–3989 (2010).
[26]H. C. Roters, *Electromagnetic Devices* (Wiley, New York, 1944), Vol. 1.
[27]T. T. Overboom, J. W. Jansen, and E. A. Lomonova, IEEE Trans. Magn. **46**(6), 2128–2131 (2010).
[28]T. Van Tran, J.-L. Coulomb, B. Delinchant, O. Chadebec, N. H. Vrijsen, J. W. Jansen, and E. A. Lomonova, in *Proceedings of the COMPUMAG, Sydney, Australia*, 2011 (Curran Associates, Inc., 2012).
[29]N. H. Vrijsen, J. W. Jansen, and E. A. Lomonova, in Proceedings of the IEEE ECCE 2012, Raleigh, NC (IEEE, 2012).
[30]G. Gautschi, *Piezoelectric Sensorics: Force, Strain, Pressure, Acceleration and Acoustic Emission Sensors, Materials and Amplifiers* (Springer, 2002).
[31]C. Lee, T. Itoh, R. Maeda, and T. Suga, Rev. Sci. Instrum. **68**, 2091 (1997).
[32]A. Albrecht, S. S. Park, Y. Altintas, and G. Pritschow, Int. J. Mach. Tools Manuf. **45**(9), 993–1008 (2005).
[33]M. Piska, L. Yang, M. Reed, and M. Saleh, J. Bone Joint Surg. Br. **84**(1), 137–140 (2002).
[34]K. Hoffmann, *An Introduction to Measurements using Strain Gages: With 172 Figures and Tables* (Hottinger Baldwin Messtechnik GmbG, 1989).
[35]A. Goldman, *Modern Ferrite Technology*, 2nd ed. (Springer, Pittsburgh, PA, USA, 2006), pp. 37–38.